communications biology

A Nature Portfolio journal

Article

https://doi.org/10.1038/s42003-026-10151-w

Multi-omics dissection of heat stress reveals *CIITA* as a central regulator of metabolic thermotolerance in cattle (*Bos taurus*)

Chengli Liu[1,2], Pengcheng Ruan[1], Zixuan Wang[1], Yongfu Huang[1], Lupei Zhang[3], Dawei Yu[3], Dejun Huang[4], Simone Ceccobelli[5], Huijiang Gao[3] ✉ & Guangxin E[1] ✉

Climate-driven heat stress disrupts metabolic homeostasis in livestock, yet the molecular mechanisms underlying adaptive responses remain poorly understood. Here, we integrated newly generated plasma metabolomic data from 111 heat-stressed cows with previously published whole-genome sequencing datasets from the same animals, identifying 30 metabolic markers and 27 copy number variations (CNVs) associated with 25 candidate genes involved in the regulation of these metabolites. Notably, a CNV hotspot encompassing *CIITA* emerged as a key pleiotropic locus strongly associated with acylcarnitine levels, body weight, and rectal temperature. Heat exposure suppressed *CIITA* expression in skeletal muscle, correlating with impaired myogenic development. We demonstrate that *CIITA* overexpression in vitro induces coordinated remodeling of cell cycle–related gene expression and partially alleviates heat-induced inhibition of myoblast proliferation. Moreover, *CIITA* overexpression markedly suppresses long-chain fatty acid β-oxidation and mitochondrial electron transport activity, accompanied by reduced adenosine triphosphate production, suggesting that *CIITA* may limit metabolic heat generation by constraining mitochondrial metabolic flux. Overall, these findings position *CIITA* as a central integrative regulator linking immune function, energy metabolism, and cell proliferation during bovine adaptation to heat stress, and highlight a potential genetic target for improving thermotolerance in livestock.

Heat stress poses a significant threat to livestock health and welfare, compromising animal productivity, product quality, and causing substantial economic losses. The detrimental effects of heat stress are being progressively exacerbated by ongoing climate change[1,2]. Under the state of heat stress, livestock regulate body temperature constancy by elevated respiratory rates, enhanced sweat secretion, and increased cutaneous blood flow[3]. Notably, the relatively thick subcutaneous fat layer and underdeveloped sweat glands in cattle result in compromised heat dissipation capacity, rendering them particularly susceptible to high-temperature environments[4,5]. This physiological characteristic leads to marked declines in dry matter intake, a reduction in rumination frequency, and inhibition of the digestion and absorption of nutrients[6,7]. Concurrently, heat stress induces physiological abnormalities including elevated rectal temperature and accelerated heart rate, which significantly compromise health status and production performance[8].

Maintenance of stable body temperature represents a fundamental physiological mechanism for organisms to preserve dynamic metabolic equilibrium and energy homeostasis, serving as a critical indicator of internal environmental stability[9]. During heat stress exposure, animals exhibit significant elevation of rectal temperature, which disrupts thermoregulatory homeostasis and profoundly influences systemic metabolic processes[10]. As terminal products of cellular physiological activities, metabolites serve as highly sensitive biomarkers reflecting the adaptive metabolic responses and regulatory states under thermal challenge[11]. Notably, metabolites are not only

[1]College of Animal Science and Technology, Southwest University, Chongqing, China. [2]College of Biology and Food Engineering, Chongqing Three Gorges University, Chongqing, China. [3]Institute of Animal Sciences, Chinese Academy of Agricultural Sciences, Beijing, China. [4]Chongqing Vocational College of Agriculture, Chongqing, China. [5]Department of Agricultural, Food and Environmental Sciences, Università Politecnica delle Marche, Ancona, Italy.
✉e-mail: gaohuijiang@caas.cn; eguangxin@126.com

the terminal products of genetic information expression, but also actively participate in regulating cellular functions, thereby constructing a sophisticated bidirectional regulatory network between genetic expression and metabolic pathways[12]. For instance, L-theanine demonstrates protective effects against heat-induced protein toxicity and metabolic dysregulation through modulation of the Hsf1/AMPK signaling pathway[13]. Recent investigations have shown that heat stress upregulates the expression of the *CASTOR1* gene, activating the mTORC1 signaling pathway and subsequently enhancing mitochondrial oxidative phosphorylation function via the mTORC1/PGC-1α/NRF1 axis, thereby improving cellular thermal adaptation[14]. Furthermore, the natural antioxidant metabolite S-allyl cysteine has been shown to mitigate heat stress-induced oxidative damage in mammary epithelial cells through activation of the Nrf2/HO-1 pathway, demonstrating significant cytoprotective effects[15]. These findings collectively suggest that metabolites regulate cellular homeostasis, especially mitochondrial function, via pathway-specific modulations, with homeostasis maintenance being essential for cellular energy metabolism and redox balance[16]. Nevertheless, the metabolic responses in heat stressed beef cattle remain poorly understood, with key gaps persisting in identifying critical biomarkers and elucidating genetic regulatory mechanisms. Systematic studies are needed to decode the molecular networks governing bovine thermal adaptation.

The advancement of metabolomics has established metabolite-based genome-wide association studies (GWAS) as a key strategy for deciphering metabolic pathways and genetic regulation of complex animal traits[17]. This approach links genotypes to production traits through metabolite intermediaries, identifying genes controlling critical metabolic nodes to reveal phenotypic mechanisms[18]. As major genomic structural variations, copy number variations (CNVs) collectively surpass SNPs and InDels in genomic impact and functional significance[19,20]. Numerous studies have shown that CNVs modulate gene networks through copy number alteration, regulatory region remodeling, and chromatin architecture modification[21–23]. For instance, *KRAS* copy number gain directly triggers *KRAS* pathway hyperactivation, disrupting glycolysis, lipid metabolism, and redox balance[24]. While primarily demonstrated in humans and mice, these mechanisms inform CNV-mediated metabolic network studies in ruminants.

This study represents a continuation of our previous work and integrates newly generated plasma metabolomics data with previously published whole-genome sequencing (WGS) data (CNV-based GWAS) from the same population. By explicitly combining these existing genomic datasets with newly generated metabolomic profiles, we systematically identify metabolic markers and regulatory genes associated with heat stress adaptation in cattle. Through integrative analyses of these multi-omics data, we further elucidate the molecular interaction networks underlying thermotolerance. These findings provide precise molecular targets for breeding strategies aimed at improving climate resilience and promoting sustainable beef production under global warming.

Results

The association between heat stress and daily weight gain in cattle

The temperature–humidity index (THI) measurements at the cattle farm indicated mild heat stress (THI 73–79) during the morning (08:00) and evening (22:00), and moderate heat stress (THI 79–89) in the afternoon (15:00) (Fig. 1A). To further elucidate the physiological basis of seasonal variation, we analyzed the relationship between average daily gain and physiological indicators in adult Huaxi cattle under heat stress (Fig. 1B). In adult cattle, rectal temperature was significantly negatively correlated with relative daily weight gain ($P = 0.0001$, $r = -0.3777$; Fig. 1C). In addition, the average daily gain of calves from July to September was lower than that from September to October ($P < 0.01$; Supplementary Fig. 1). These results suggest that elevated body temperature may adversely affect growth performance.

Influence of heat stress on peripheral blood metabolism

Plasma metabolomic profiling of 111 heat stressed cows identified 852 metabolites. Differential abundance analysis comparing 20 high-rectal-temperature (≥39.3 °C) and 20 low-rectal-temperature (≤38.7 °C) individuals identified 97 significantly altered metabolites, including 3-oxodecanoic acid and multiple carnitine derivatives (Fig. 2A, B). Weighted gene co-expression network analysis (WGCNA) grouped these metabolites into seven co-expression modules (Fig. 2C). Among them, the turquoise and brown modules showed significant correlations with rectal temperature ($P < 0.01$; Fig. 2D) and contained 218 metabolites, including carnitine C18:1 and hexanoyl glycine. Intersection of WGCNA-derived metabolites with differentially abundant metabolites resulted in 83 consensus heat-responsive metabolites. Pearson correlation analysis further prioritized the top 30 marker metabolites (MMTs; Supplementary Table 1), consisting of 23 acylcarnitines, 3 amino acid derivatives, 1 glycerophospholipid, and 3 organic acid derivatives. Kyoto Encyclopedia of Genes and Genomes (KEGG) enrichment analysis showed that MMTs were predominantly associated with pathways involved in thermogenesis and lipid metabolism (Fig. 2E). Notably, 23 acylcarnitines—including carnitine C10:0 and C11:1—were enriched in thermogenesis-related pathways, suggesting a potential regulatory role in maintaining thermal homeostasis under heat stress.

Screening candidate genes based on metabolism-genomic association analysis

A total of 33,078 high-confidence CNVs were identified from the genome resequencing data of 111 cows. Comparative analysis of multiple GWAS models indicated that the BLINK model outperformed others in terms of consistency between expected and observed associations (Supplementary Fig. 2). Accordingly, BLINK was employed to perform GWAS on 30 MMTs using a significance threshold of $P \le 1.51 \times 10^{-6}$. This analysis identified significant associations between 16 MMTs—such as carnitine C16:0, C18:0, and 3-Oxodecanoic acid—and 27 CNVs, resulting in the annotation of 25 candidate genes (Supplementary Fig. 3). Notably, a CNV located within the *CIITA* gene (CHR25:9,557,000–9,605,500 bp) was significantly associated with four MMTs (carnitine C14:1, C16:0, C18:0, and C18:1; Fig. 3A), implicating its involvement in heat stress-related metabolic regulation.

Functional enrichment analysis revealed that the candidate genes were enriched in pathways including nicotinate and nicotinamide metabolism, carbohydrate metabolism, and the insulin signaling pathway (Fig. 3B), as well as in biological processes such as cellular response to heat, mitochondrial electron transport, and energy homeostasis (Fig. 3C). Collectively, these findings suggest that CNV-associated genes play pivotal roles in metabolic remodeling and adaptive responses under heat stress, highlighting CNVs as critical genomic determinants of metabolic adaptation in cattle.

Relationship between the CIITA gene and the growth and development of cattle

To assess the responsiveness of candidate genes to heat stress and their tissue-specific expression patterns, we performed transcriptomic profiling across multiple tissues under heat-stressed and thermoneutral conditions. Sixteen candidate genes showed significant differential expression in response to heat stress (Fig. 4A), with *CIITA* and *AOX1* showing the most pronounced changes in skeletal muscle.

To contextualize these heat-responsive changes within muscle development, we compared longissimus dorsi transcriptomes from young and adult cattle under thermoneutral conditions. *CIITA* expression was significantly higher in adult than in young cattle (FDR < 0.01; Fig. 4B), indicating that its expression is closely associated with muscle maturation. Taken together, these results indicate that heat stress–induced downregulation of *CIITA* occurs in a gene that is normally highly expressed in mature muscle, suggesting that its suppression may coincide with transcriptional features associated with impaired myogenic development.

CNV analysis of *CIITA* across 202 individuals identified three genotypes: biallelic normal (-/-), heterozygous duplication (−/+), and homozygous duplication (+/+). The identified CNV encompasses exons 2–20 and the 3′UTR of *CIITA* gene (Fig. 4C), with validation through read-depth

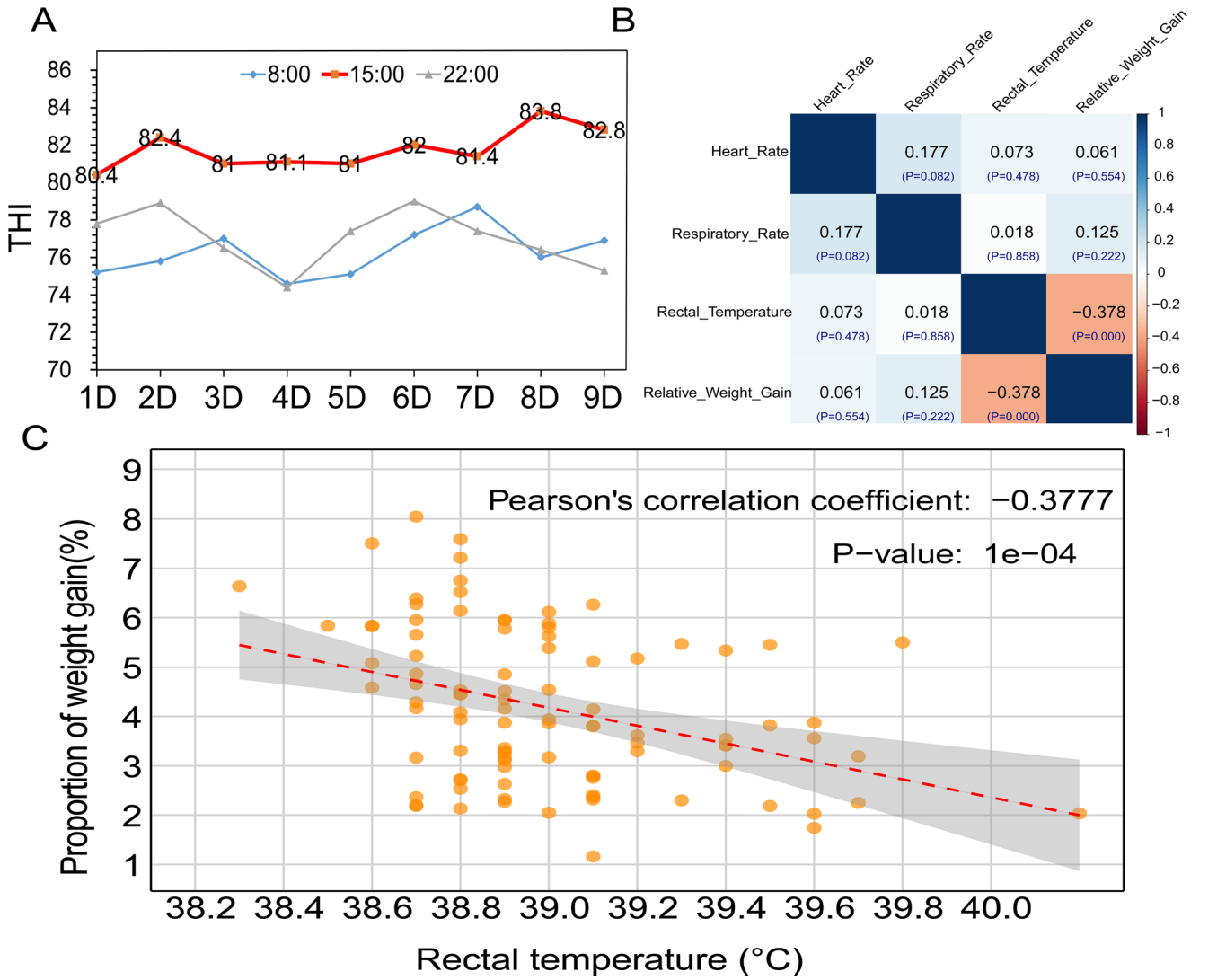

Fig. 1 | Heat stress impairs the growth performance of Huaxi cattle. A Changes in the THI at three time points per day over a 9-day period during sample collection. **B** This heatmap illustrates the correlations among rectal temperature, respiratory rate, heart rate, and relative daily weight gain in 111 Huaxi cattle under high-temperature conditions. **C** This scatter plot illustrates the correlation between rectal temperature (August 2–4) and relative daily weight gain (July–September) in 111 Huaxi cows, with a correlation coefficient of −0.3777 and a significance level of $P = 1 \times 10^{-4}$.

analysis and real-time quantitative polymerase chain reaction (qPCR, Fig. 4D, E). Biallelic normal (-/-) individuals demonstrated significantly increased body weights relative to heterozygous counterparts at 18 months ($P = 0.009$) and 24 months ($P = 0.042$), accompanied by a trend toward larger longissimus dorsi muscle cross-sectional areas (Fig. 4F). Notably, *CIITA* genotypes exhibited significant divergence in rectal temperature regulation during heat stress ($P = 0.039$, Fig. 4G). These results suggest that *CIITA* CNV may regulate thermoregulation and muscle development under heat stress, highlighting its potential as a valuable genetic marker for improving heat tolerance in cattle breeding programs.

Construction of a heat stress model in cattle skeletal muscle satellite cells (SMSCs)

Primary bovine SMSCs were successfully isolated (Fig. 5A), and PAX7 immunofluorescence confirmed a high cellular purity (>94%) (Fig. 5B). Establishment of the heat stress model showed that expression levels of *HSP60* and *HSP70* peaked after 3 h of exposure to 42 °C, identifying this condition as optimal for inducing a robust heat stress response (Fig. 5C). Heat stressed SMSCs displayed markedly reduced proliferative capacity ($P < 0.01$; Fig. 5D), accompanied by significant downregulation of proliferation markers *CDK2* and *PCNA* ($P < 0.01$). In parallel, the expression of mitochondrial dynamics regulators (*FIS1*, *MFN1*, *MFN2* and *DRP1*) was significantly altered following heat exposure ($P < 0.05$; Fig. 5F). Notably, *CIITA* expression was substantially reduced under heat stress ($P < 0.05$), suggesting its potential involvement in modulating the cellular heat stress response (Fig. 5F).

CIITA regulates the cell cycle and alleviates the inhibition of cell proliferation caused by heat stress

In this study, adenoviral vectors for *CIITA* overexpression and knockdown were constructed in SMSCs (Fig. 6A). QPCR analysis confirmed the successful overexpression and knockdown of *CIITA* in SMSCs (Fig. 6B). Transcriptomic profiling of *CIITA* overexpressing SMSCs under heat stress identified 1713 differentially expressed genes (DEGs), with pronounced upregulation of antigen presentation-related genes (*BOLA-DRA*, *BOLA-DQB*, and *CD74*; Fig. 6C). QPCR validation confirmed that *CIITA* overexpression and knockdown were consistent with the RNA-seq results, supporting the reliability of the transcriptomic analysis (Fig. 6D). Functional enrichment analysis showed that DEGs were significantly enriched in multiple signaling pathways such as cell cycle, DNA replication, thermogenesis, and antigen processing and presentation (Fig. 6E). Gene Ontology (GO) analysis results also showed that terms such as cell division, mitotic

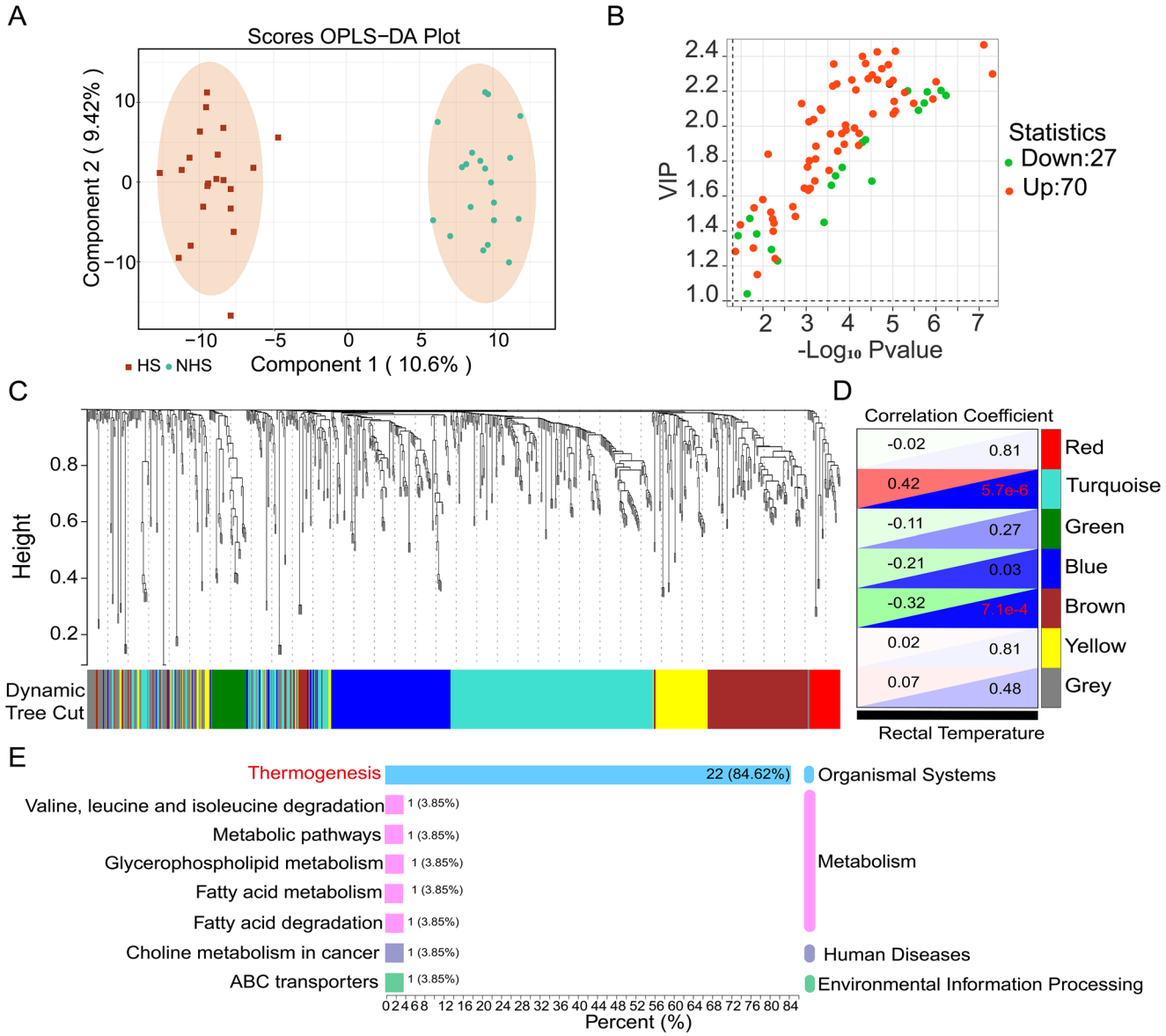

Fig. 2 | Identification and functional enrichment analysis of MMTs (marker metabolite loci) in 111 cattle. A OPLS-DA (orthogonal partial least squares discriminant analysis) of metabolites between heat stress (HS) and non-heat stress (NHS) groups ($n = 20$). **B** Volcano plot of differential metabolites between HS and NHS groups. **C** Metabolite clustering dendrogram generated by WGCNA. Each leaf represents a metabolite, and the color bars below indicate module assignments. **D** Heatmap showing correlations between metabolite modules and rectal temperature. **E** KEGG pathway enrichment analysis of MMTs.

sister chromatid segregation, nucleoplasm, and ATP binding were significantly enriched (FDR < 0.01, Fig. 6F).

Notably, 42 of 44 cell cycle-related DEGs showed marked upregulation (Fig. 6G). Protein–protein interaction (PPI) network analysis suggested *CIITA* regulates cell cycle progression via *CREBBP*-mediated modulation of *PCNA*, *CDK1*, and *CCND1* (Fig. 6H). Consistently, *CIITA* overexpression increased *CREBBP* expression and enhanced cell cycle progression under heat stress, as evidenced by reduced G0/G1 phase cells and elevated S/G2/M phase populations (Fig. 6I). These findings demonstrate that *CIITA* mitigates heat stress-induced proliferation arrest and cell cycle inhibition.

The influence of heat stress on the activity and proliferation of SMSCs

To investigate the role of *CIITA* in SMSCs under heat stress, we assessed cell viability and proliferation. *CIITA* overexpression significantly increased the viability of SMSCs under both thermoneutral and heat stress conditions ($P < 0.01$), with further enhancement observed during prolonged heat exposure ($P < 0.01$). Conversely, *CIITA* knockdown severely impaired viability ($P < 0.01$, Fig. 7A). EdU assays confirmed these trends: *CIITA* overexpression markedly enhanced proliferation across conditions, while its knockdown caused significant suppression (Fig. 7B). These results indicate that *CIITA* enhances cellular activity and promotes proliferation.

CIITA regulates cellular energy homeostasis under heat stress via metabolic remodeling

To elucidate the metabolic role of *CIITA* during heat stress, we performed untargeted metabolomic profiling of *CIITA* overexpressing SMSCs. Orthogonal partial least squares discriminant analysis (OPLS-DA) analysis revealed clear separation of metabolite profiles between *CIITA*-overexpressing and control cells. A total of 610 metabolites were detected (Fig. 8A), of which 59 were differentially abundant, including 41 upregulated and 18 downregulated metabolites. Notably, three long-chain acylcarnitines—C16:0, C18:0, and C18:1—previously identified in CNV–metabolite GWAS were significantly elevated in *CIITA*-overexpressing cells (Fig. 8B). Functional enrichment analysis associated these metabolites with thermogenic pathways (Fig. 8C). Transcriptomic profiling

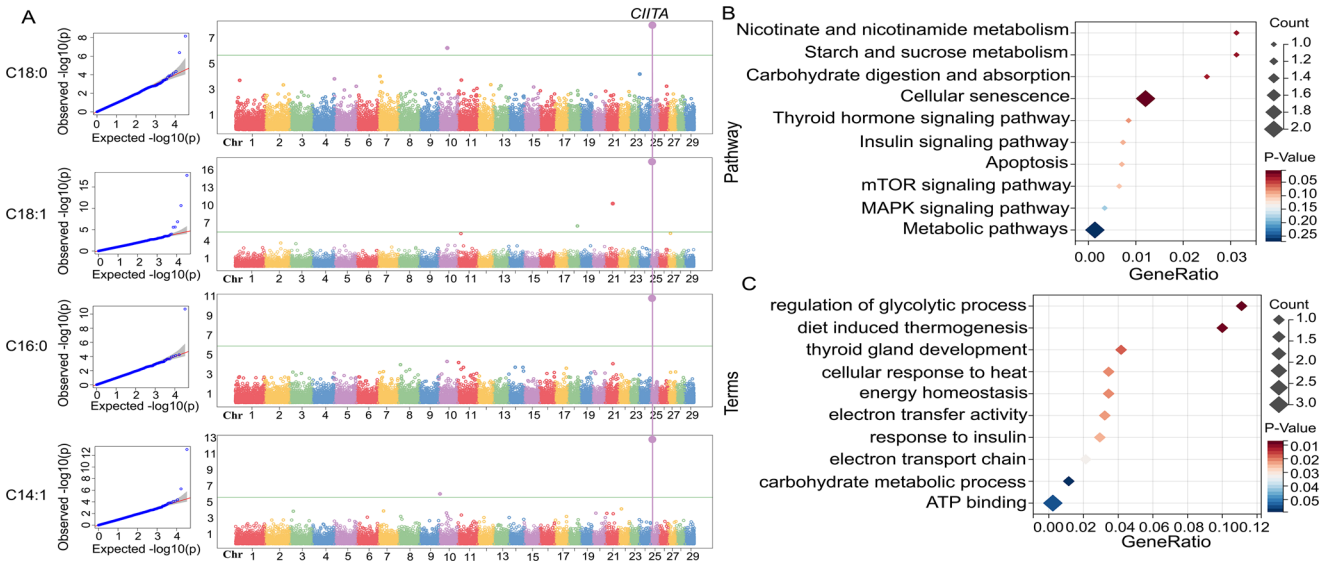

Fig. 3 | GWAS of MMTs in 111 cows and functional enrichment analysis of the candidate genes. A GWAS results using MMTs as phenotypic traits. Left: QQ plot for a representative locus (CHR25:9,557,000–9,605,500 bp); Right: corresponding Manhattan plot. **B** KEGG pathway enrichment analysis of candidate genes. **C** GO functional enrichment analysis of candidate genes.

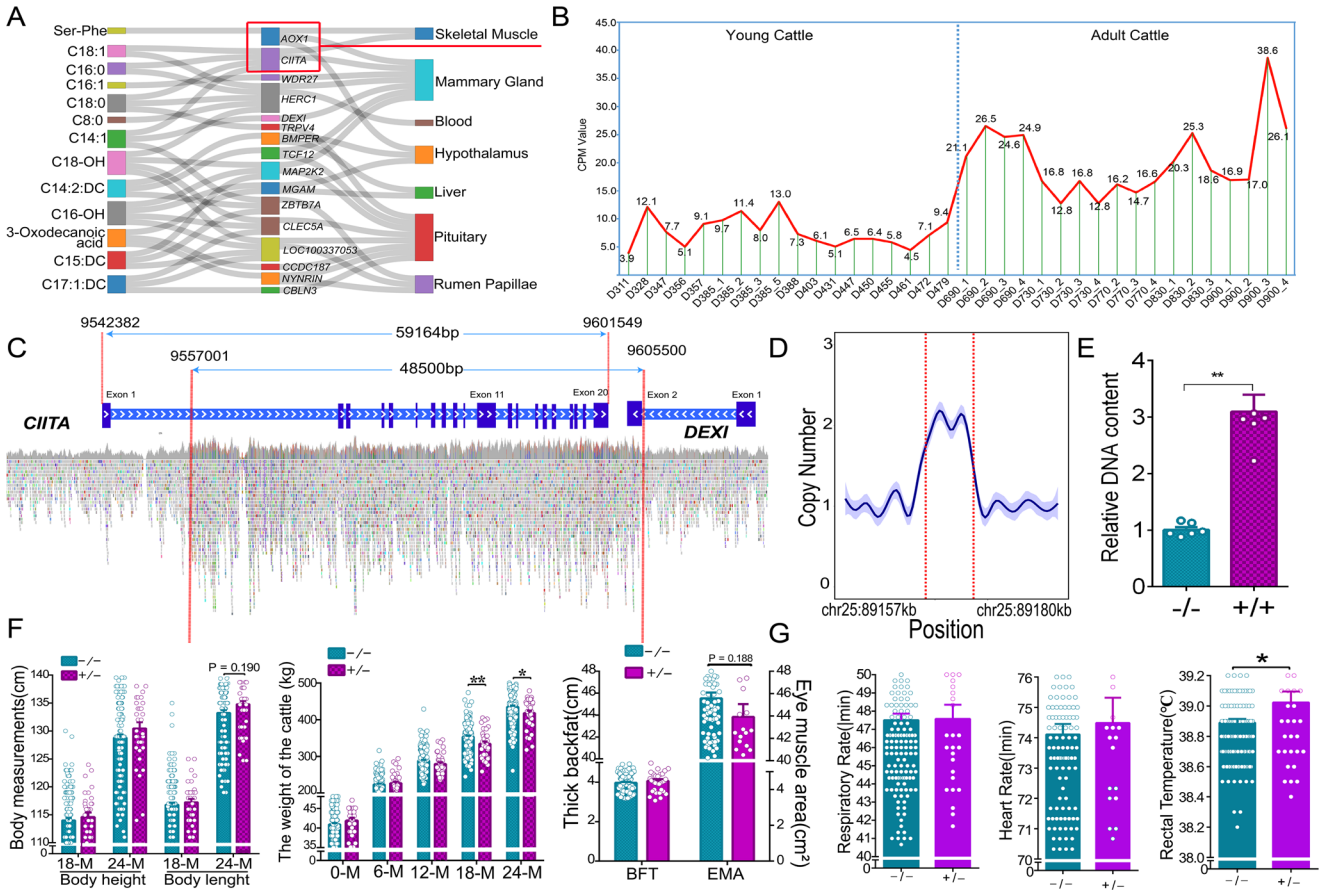

Fig. 4 | Correlation of *CIITA* gene CNV with growth traits in cattle. A Expression patterns of heat stress-related candidate genes across tissues (Sankey plot). **B** Age-dependent expression of the *CIITA* gene in the longissimus dorsi muscle of young and adult cattle. The y-axis represents expression levels, and the x-axis indicates age in days ($n = 18$ per group). **C** Close-up IGV screenshots of Illumina short-read sequences aligned to the *CIITA* locus. **D** Genomic read coverage across different genotypes. **E** qPCR validation of DNA copy number across CHR25:9,557,000–9,605,500 bp in cattle with different genotypes. **F** Comparison of body size, body weight, backfat thickness, and longissimus dorsi muscle area among different genotypes in 202 cattle. **G** Physiological parameters (respiratory rate, heart rate, and rectal temperature) under heat stress across genotypes. Note: -/- indicates biallelic normal; −/+ indicates heterozygous duplication; +/+ indicates homozygous duplication ($n = 202$).

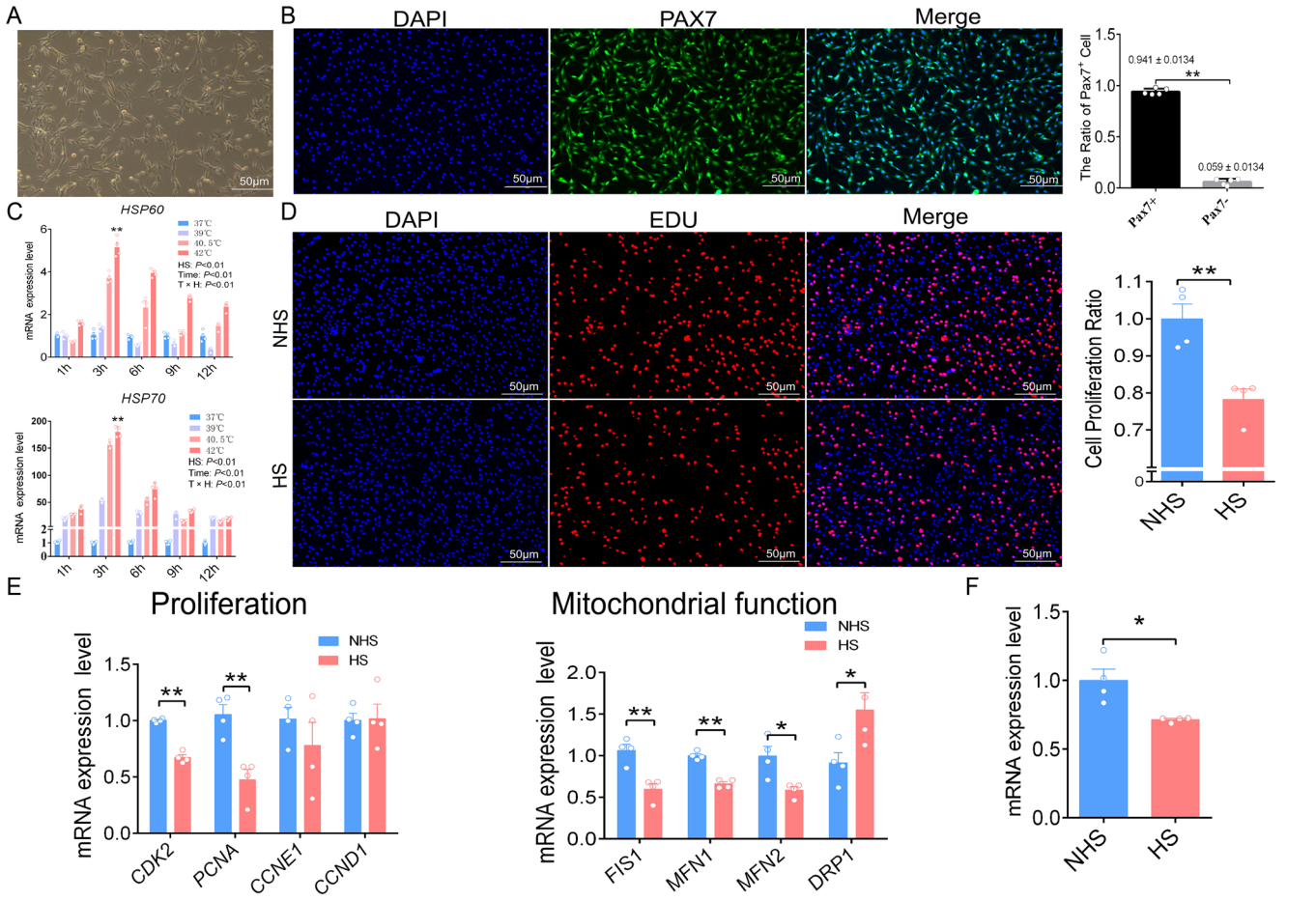

Fig. 5 | Heat stress significantly affects proliferation, mitochondrial function, and *CIITA* gene expression in primary SMSC. A Morphology of primary bovine SMSCs. **B** Immunofluorescence staining of the specific marker PAX7, indicating SMSCs identity ($n = 5$). **C** Expression patterns of *HSP60* and *HSP70* under various heat stress temperatures and durations. **D** EdU assay showing the proliferation rate of SMSCs under heat stress (HS) and non-heat stress (NHS) conditions ($n = 4$). **E** Expression analysis of genes related to cell proliferation, and mitochondrial function. **F** *CIITA* gene expression in SMSCs in response to heat stress stimulation.

further revealed that *CIITA* overexpression altered the expression of 34 genes within the thermogenesis pathway, with 31 being downregulated, including the fatty acid activation enzymes *ACSL4* and *ACSL6*. Concurrently, genes encoding mitochondrial electron transport chain components—NADH dehydrogenase, ubiquinol–cytochrome c reductase, cytochrome c oxidase, and ATP synthase—were also significantly suppressed (FDR < 0.05; Fig. 8D). Consistently, ATP quantification assays demonstrated that *CIITA* overexpression significantly decreased intracellular ATP levels ($P < 0.01$), whereas *CIITA* knockdown significantly increased ATP levels ($P < 0.05$; Fig. 8E). Collectively, these findings indicate that *CIITA* reprograms cellular metabolism under heat stress by suppressing long-chain fatty acid activation and mitochondrial oxidative phosphorylation, resulting in accumulation of acylcarnitines, likely due to impaired β-oxidation (Fig. 8F). This metabolic remodeling potentially acts as an adaptive mechanism to alleviate heat-induced metabolic stress while maintaining energy homeostasis in muscle cells.

Discussion

Heat stress is a major challenge in the livestock industry, adversely affecting not only animal health and welfare but also productivity and the genetic progress of breeding populations. In this study, we observed that heat stress significantly suppressed daily weight gain in beef cattle. Concurrently, heat stress was associated with elevated rectal temperatures, which negatively correlated with relative daily weight gain. These findings are consistent with previous reports. For instance, in environments characterized by high temperature and humidity, cattle exhibited a 12% reduction in dry matter intake and approximately a 23% increase in water intake[25]. Furthermore, heat stress during late gestation in dairy cows not only increases their physiological burden but also leads to long-term developmental deficits in their offspring, primarily manifested as reduced birth weight, smaller weaning size, and lower body weight and height at 12 months compared to calves not exposed to prenatal heat stress[26]. Briefly, the heat stress elevates core body temperature, increases internal heat load, and initiates a cascade of physiological stress responses and energy metabolism disruptions[27].

In this study, we identified a significant increase in acylcarnitine metabolites in the peripheral blood of cattle exposed to heat stress. Acylcarnitines, conjugates of carnitine and acyl-CoA, play a critical role in transporting fatty acids from the cytoplasm into the mitochondrial matrix, where they undergo β-oxidation[28]. Under physiological conditions, acylcarnitines are transported across the mitochondrial membrane via the carnitine palmitoyltransferase I/II (CPT I/II) system, where they are deacylated and converted back into acyl-CoA for subsequent oxidation[29]. However, previous studies have shown that heat stress can impair CPT II function, thereby hindering mitochondrial fatty acid oxidation and leading to the accumulation of long-chain acylcarnitines, such as palmitoylcarnitine[30,31]. Consequently, the elevated levels of acylcarnitines observed under heat stress may reflect a disruption in mitochondrial fatty acid metabolism and an imbalance in energy supply and demand, representing a metabolic response to heat-induced cellular injury.

Previous studies have demonstrated that approximately 50% of the phenotypic variation in metabolite levels can be attributed to underlying genetic variation[32], suggesting that inter-individual differences in

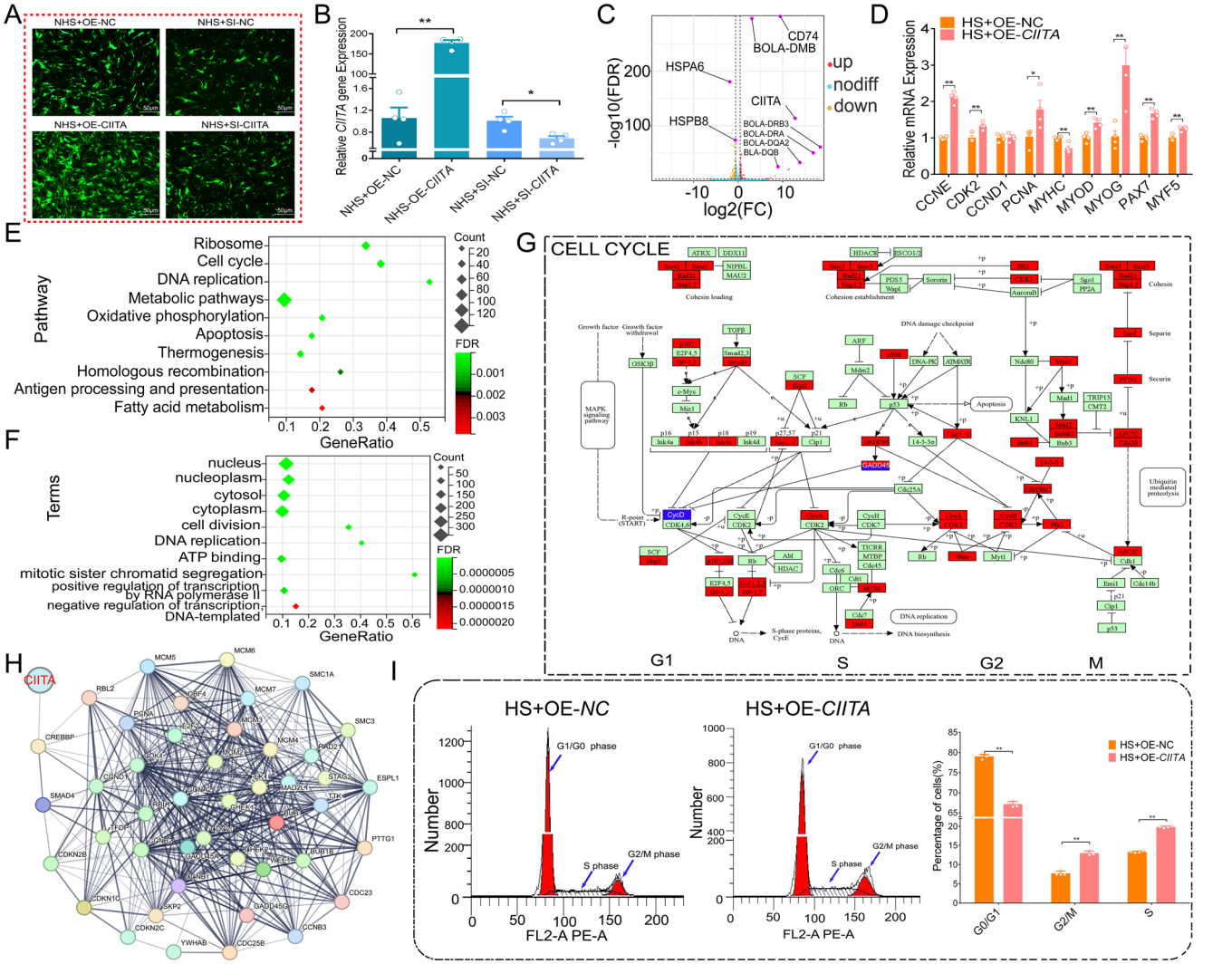

Fig. 6 | *CIITA* overexpression alters the cell cycle distribution of SMSCs under heat stress via modulation of cell cycle genes. A Fluorescence images of overexpression and knockdown cells; **B** Relative expression levels of *CIITA* gene in overexpression and knockdown cells. **C** Volcano plot of DEGs. Red dots indicate significantly upregulated genes, yellow dots indicate significantly downregulated genes, and blue dots represent non-significant genes. **D** Validation of transcriptomic data by qPCR. **E** KEGG enrichment analysis of DEGs. **F** GO enrichment analysis of DEGs. **G** Cell cycle signaling pathway map. Red indicates significant upregulation, blue indicates significant downregulation, and light green indicates no significant difference. **H** PPI network of DEGs (partial view). **I** Flow cytometry analysis of cell cycle distribution in SMSCs overexpressing *CIITA* ($n = 4$).

metabolic traits are not solely shaped by environmental influences but are also strongly modulated by genetic background. In this study, GWAS based on MMTs identified 27 CNVs and 25 candidate genes, including *HERC1*, *CIITA*, and *MGAM*. Functional enrichment analyses revealed that these genes are primarily involved in key metabolic and endocrine pathways, such as thyroid hormone synthesis, insulin secretion, and carbohydrate and mineral absorption. Among these, thyroid hormone plays a pivotal role in regulating basal metabolic rate and thermogenesis. Its biosynthetic regulation is closely associated with the organism's ability to adapt to metabolic demands under thermal stress[33]. Reducing thyroid hormone levels can help lower endogenous heat production, thereby enhancing thermal tolerance in high-temperature environments[34]. The enrichment of the insulin signaling pathway further indicates that heat stress may impair glucose metabolism and disrupt systemic energy allocation, ultimately affecting nutrient regulation and insulin sensitivity[35–37]. By modulating insulin secretion, it is possible that animals optimize energy utilization and maintain essential physiological processes under thermal stress[38]. A substantial number of candidate genes were also enriched in pathways related to carbohydrate and mineral digestion and absorption, highlighting the dual challenges imposed by heat stress on both energy supply and electrolyte balance[39,40]. Essential minerals such as sodium, potassium, and calcium are crucial for maintaining cellular homeostasis and neuromuscular function, and disturbances in their absorption may reduce the animals' resilience to thermal stress[41]. Collectively, these findings suggest that the identified candidate genes contribute to the adaptive response to heat stress through the coordinated regulation of hormone secretion, energy metabolism, and nutrient absorption.

Notably, we observed that many candidate genes identified under heat stress conditions were differentially expressed across multiple tissues, with the pituitary gland exhibiting the highest number of DEGs. This may be attributed to the pituitary's pivotal role as one of the most critical neuroendocrine organs in animals, orchestrating a wide range of physiological processes including metabolism, development, reproduction, and immune function. Given its central regulatory function, the pituitary is likely more sensitive to environmental stressors such as heat. Moreover, several of these candidate genes have been previously implicated in heat stress adaptation in various tissues and organs. For instance, *AOX1* has been identified as a key regulator of the heat stress response in bovine ovarian granulosa cells, supported by integrative transcriptomic and metabolomic analyses[42], and is

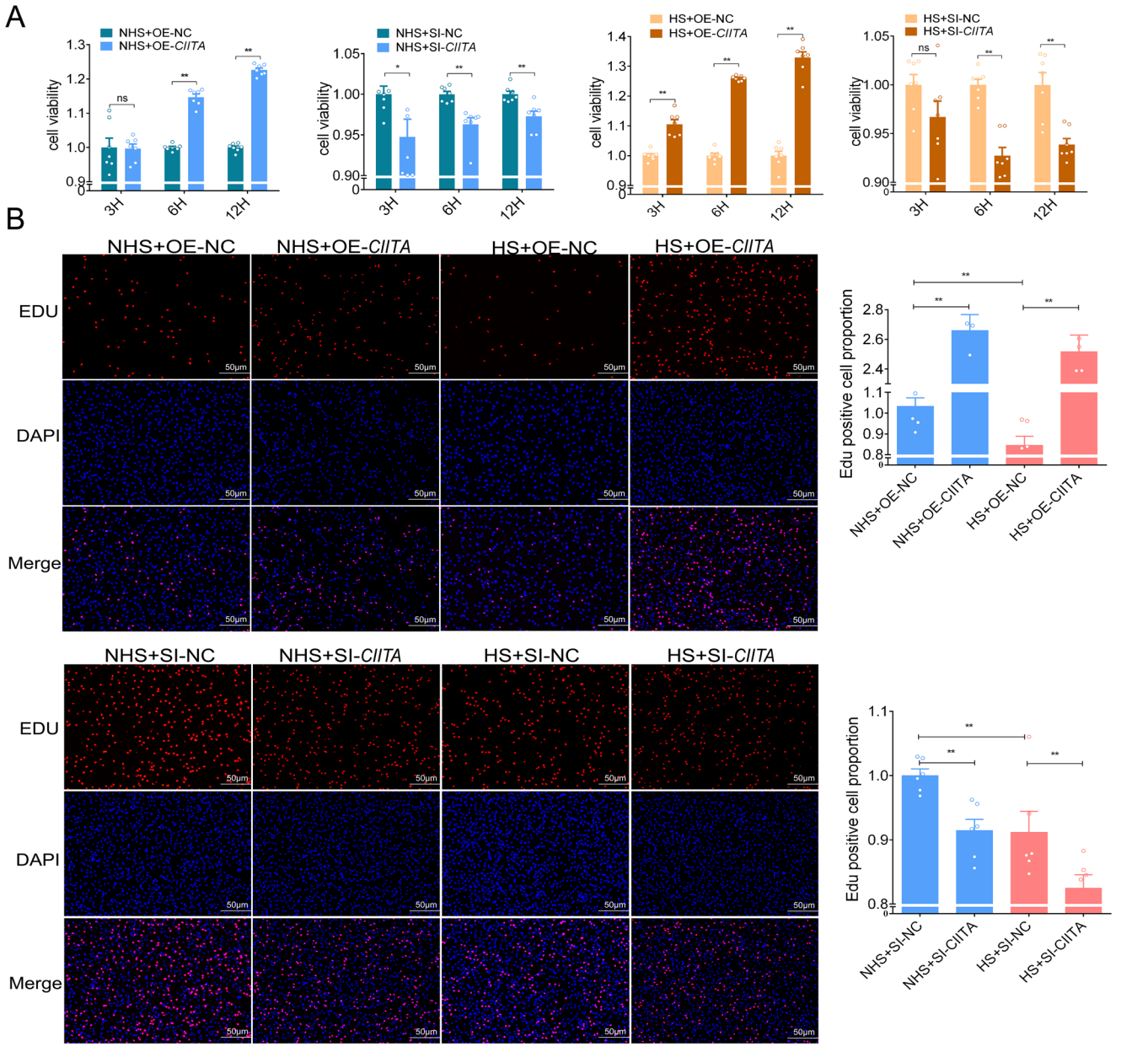

Fig. 7 | Overexpression of *CIITA* enhances cell viability and proliferation of SMSCs under both heat stress and normal temperature conditions. A Cell viability of *CIITA* overexpressing or knockdown SMSCs was assessed using the CCK-8 assay after 3, 6, and 12 h of heat stress or thermoneutral treatment ($n = 7$). **B** EdU assay showing the proliferation of *CIITA* overexpressing or knockdown SMSCs under heat stress or thermoneutral conditions, along with quantification of EdU positive cells ($n = 6$).

also involved in mediating the gut microbiota's response to thermal stress in cattle[43]. Importantly, *AOX1* has also been repeatedly reported as a conserved heat-responsive gene across diverse plant species, including Forsythia, soybean, and maize, as well as in microorganisms[44–46], suggesting that *AOX1* may play an evolutionarily conserved role in heat stress tolerance across species. In addition, *CIITA* was significantly upregulated in the lung tissues of Cherry Valley ducks under heat stress and has been proposed as a central regulator of immune activation and cellular stress responses[47]. Furthermore, *MGAM* has been shown to participate in starch and sucrose metabolism during high-temperature stress in oil palm seeds, acting as a crucial metabolic regulator during heat stress adaptation in plants[48]. In summary, the candidate genes identified in this study are not only involved in heat stress adaptation in cattle but have also been consistently validated in multiple tissues and species. These results indicate that many of these genes may serve as evolutionarily conserved regulators of heat stress responses and likely play pivotal roles in the genetic mechanisms underlying thermotolerance in cattle.

Importantly, we found that two candidate genes, *AOX1* and *CIITA*, were differentially expressed in bovine muscle tissue under heat stress conditions. *CIITA* showed significantly higher expression in the muscle tissue of adult cattle, and adult body weight varied significantly among individuals with different *CIITA* genotypes. These findings suggest that *CIITA* may serve as a potential candidate gene associated with muscle growth and development under heat stress, and that CNVs within this gene could be related to the impact of thermal stress on bovine growth performance.

Notably, the present study observed that overexpression of *CIITA* in bovine SMSCs was associated with significant changes in the expression of several immune- and metabolism-related genes, including *IL-6*. Previous studies have reported that *CIITA* overexpression can suppress *IL-6*, a pro-

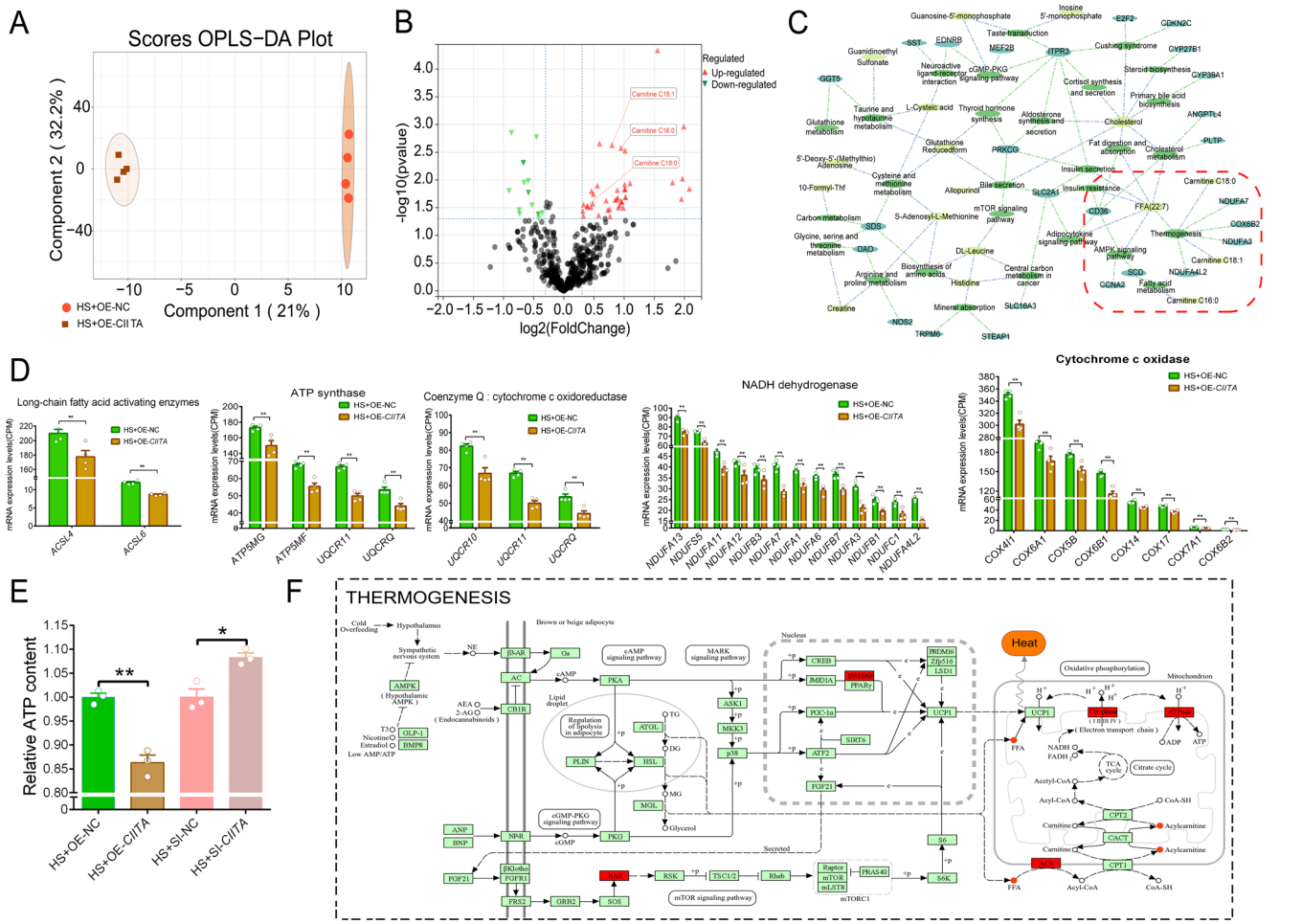

Fig. 8 | Under heat stress, *CIITA* overexpression leads to a reduction in ATP production by suppressing mitochondrial oxidative phosphorylation. **A** OPLS-DA analysis of the SMSCs metabolomic profiles ($n = 4$). **B** Volcano plot of differentially expressed metabolites. **C** Integrated network analysis of DEGs and metabolites. The red region highlights DEGs and metabolites involved in thermogenesis pathways. **D** Expression changes of genes related to long-chain fatty acid activation, ATP synthase, NADH dehydrogenase, cytochrome c oxidase, and ubiquinol-cytochrome c reductase. **E** Relative ATP content determination ($n = 3$). **F** DEGs and metabolites in the thermogenesis-related signaling pathway of *CIITA* overexpressing SMSCs under heat stress. Red indicates significantly altered molecules.

inflammatory cytokine implicated in cellular stress responses and tissue stability under heat stress conditions[49,50]. In addition, *IL-6* has been independently characterized as a key myokine involved in the regulation of muscle stem cell proliferation and energy metabolism[49,51]. In the context of the present study, heat stress–induced downregulation of *CIITA* may be associated with changes in transcriptional programs relevant to muscle regeneration. However, cytokine levels were not directly measured, and the regulatory relationship between *CIITA* and *IL-6* was not experimentally examined. Therefore, further studies will be required to determine whether *CIITA* contributes to the maintenance of the muscle regenerative microenvironment during heat stress.

As the master co-activator of major histocompatibility complex (MHC) class II gene transcription, *CIITA* plays a central role in regulating MHC II expression, facilitating antigen presentation, and initiating adaptive immune responses. In the present study, *CIITA* expression was markedly downregulated under heat stress, which may result in reduced expression of MHC II molecules (e.g., *BOLA-DRB3*, *BOLA-DQB*) and consequently impair antigen presentation and adaptive immune activation[52]. This observation is consistent with previous reports showing that heat stress not only triggers heat shock responses and aberrant cytokine release but also leads to immune organ atrophy, increased lymphocyte apoptosis, and impaired antigen presentation, ultimately contributing to systemic immunosuppression[53]. Furthermore, studies in animal models have demonstrated that heat stress can downregulate MHC II expression, reducing the host's capacity to recognize and eliminate exogenous pathogens. To further verify these findings, we established a *CIITA* overexpression model in SMSCs. Overexpression of *CIITA* significantly increased the transcription of MHC class II-related genes (e.g., *BOLA-DRB3*, *BOLA-DQB*), and antigen processing and presentation pathways were notably activated. These results confirm the role of *CIITA* as a core regulatory factor in MHC class II gene expression and support its potential protective role in maintaining immune homeostasis under heat stress. Collectively, these findings highlight *CIITA* as a key mediator in the immunosuppressive response to heat stress and a potential molecular target for mitigating immune dysfunction caused by thermal challenge.

This study provides evidence suggesting that *CIITA* may be involved in the regulation of the cell cycle under heat stress conditions. Specifically, *CIITA* overexpression was associated with significant upregulation of approximately 95% (42/44) of the DEGs related to the cell cycle signaling pathway, which coincided with increased proliferative activity in SMSCs. Further analysis showed that *CIITA* overexpression was accompanied by a significant increase in *CREBBP* expression. While the direct regulatory relationship between *CIITA* and *CREBBP* was not experimentally validated in this study, previous studies have shown that *CIITA* can function as a transcriptional coactivator by recruiting multiple transcription factors and epigenetic regulators, including CREBBP, to form transcriptional complexes involved in gene regulation. For instance, previous studies have reported that *CIITA* can interact with the N-terminal region of *CREBBP* via

its transcriptional activation domain, which has been implicated in the regulation of downstream gene expression and cell cycle–related processes[54,55]. *CREBBP* can further enhance the transcriptional activity of *CCND1* through acetylation, promoting cell proliferation[56]. It may also influence *CDK1* gene accessibility by remodeling chromatin structure and regulating its transcription through interactions with key transcription factors such as FOXM1 and E2F[57–59]. Additionally, CREBBP can bind directly to the PCNA promoter, facilitating DNA replication and repair processes that collectively drive cell proliferation[60,61]. These mechanisms complement the heat stress-induced responses such as DNA damage repair, metabolic reprogramming, and cell cycle arrest[62]. Taken together, these findings suggest that *CIITA*-associated regulatory changes may be linked to enhanced cellular proliferative and repair capacity under heat stress, potentially contributing to the maintenance of tissue homeostasis; however, the specific involvement and mechanistic relationship of *CREBBP* in this process remain to be further validated in Huaxi cattle.

In this study, we found that *CIITA* overexpression not only enhanced the proliferative capacity of SMSCs and activated immune-related signaling pathways but also suppressed the activity of the mitochondrial electron transport chain and fatty acid β-oxidation. Previous studies have demonstrated that *CIITA* can activate several key immune-associated pathways, including antigen processing and presentation, the AMPK signaling pathway, and the TNF signaling pathway[63,64], all of which are closely linked to alterations in cellular energy metabolism. Notably, metabolic reprogramming has been widely recognized as a fundamental mechanism underlying cellular stress responses and proliferation control[65]. During immune cell activation—such as in T cells and macrophages—metabolism typically shifts from mitochondrial oxidative phosphorylation (OXPHOS) toward glycolysis to satisfy the increased demands for energy and biosynthetic precursors required for rapid proliferation and cytokine synthesis[66,67]. Similar metabolic features have also been reported in other rapidly proliferating cell types, including activated SMSCs[68,69]. However, although *CIITA* overexpression in our study inhibited mitochondrial OXPHOS, transcriptomic analysis revealed no significant upregulation of canonical glycolysis-related genes. This observation suggests that *CIITA* does not induce a classical metabolic switch from OXPHOS to glycolysis in SMSCs. Instead, the enhanced proliferative capacity may be attributed to transcriptional activation of cell-cycle regulators rather than a full metabolic transition. Such a state likely reflects a form of metabolic adaptation rather than a complete metabolic reprogramming, enabling cells to balance energy production, redox homeostasis, and proliferation under heat stress conditions. In summary, *CIITA* overexpression activates immune-related pathways and modulates cellular metabolism in a manner that supports SMSC activation and proliferation. As a canonical immune regulatory factor, *CIITA* may serve as a potential integrator linking immune signaling with metabolic control, thereby contributing to the maintenance of cellular energy homeostasis and proliferative balance during thermal challenge.

In conclusion, this study integrates metabolomics, genomics, and functional validation to elucidate the molecular mechanisms underlying heat stress adaptation in cattle. By identifying *CIITA* as a potential central regulatory gene, we reveal a coordinated network linking immune activation, metabolic reprogramming, and cellular proliferation in response to thermal stress. These findings provide insights into the genetic and metabolic foundations of thermotolerance, offering potential targets for genetic selection and management strategies aimed at improving heat resilience in livestock. Ultimately, this work lays a theoretical and practical foundation for enhancing animal welfare and productivity under increasingly challenging environmental conditions.

Materials and methods

Animals and sample collection

All animal procedures were approved by the Institutional Animal Care and Use Committee of Southwest University (Approval No. IACUC-20221128-02). We have complied with all relevant ethical regulations for animal use. All experimental animals were obtained from Chongqing Jinxia Animal Husbandry Co., Ltd. (30°54′N, 108°42′E; altitude 793 m). The herd comprised a total of 239 Huaxi cows, including 202 adult females (>24 months old) and 37 calves (~12 months old). All animals were maintained under standardized feeding conditions with uniform diet formulation and management practices. All animals were provided with ad libitum access to water and a uniform total mixed ration formulated according to the Nutrient Requirements of Beef Cattle, containing consistent proportions of corn silage, concentrate, and forage. Body weight was recorded at birth and 6, 12, 18, and 24 months of age, with body height and oblique length measured at 18 and 24 months. Meanwhile, ultrasound measurements of backfat thickness and longissimus dorsi muscle area were performed between the 12th and 13th ribs at 18 months. All measurements followed the Technical Specifications for Beef Cattle Performance Evaluation (NY/T 2660-2014).

Between July 30 and August 7, 2023, ambient temperature and relative humidity inside the cattle sheds were recorded three times daily (08:00, 15:00, and 22:00). The THI was calculated using the formula: $THI = (1.8 \times T + 32) - [(0.55 - 0.0055 \times RH) \times (1.8 \times T - 26)]$, where T represents ambient temperature (°C) and RH denotes relative humidity (%)[70]. To evaluate the effects of heat stress on growth performance in adult Huaxi cattle, relative daily weight gain of adult cows ($n = 202$) was calculated for the summer period from July to September. In addition, calves ($n = 37$) were weighed in 2023 (July, September, and October), and daily weight gain was calculated for the summer (July–September) and autumn (September–October) periods. During the peak heat period, physiological parameters of adult cattle ($n = 202$)—including heart rate, respiratory rate, and rectal temperature—were measured over three consecutive days (August 2–4, 2023) between 14:00 and 16:00. At the same time points, 5.0 mL of blood was collected from the tail vein of adult cows ($n = 202$). Blood samples were gently mixed, allowed to stand for 30 min, and then centrifuged at 1500 rpm for 15 min at 4 °C. The resulting plasma was aliquoted and stored at −80 °C for subsequent metabolomic analysis. Pearson correlation coefficients were calculated using R (v4.3.2).

Metabolome determination and analysis

To investigate the effects of high ambient temperature (heat stress) on metabolic responses in Huaxi cattle, plasma metabolomic analysis was conducted on a subset of 111 healthy adult cows selected from an initial cohort of 202 individuals. These animals were chosen based on their comparable age and gestational stage (approximately 220 days), to minimize potential confounding effects caused by physiological heterogeneity, particularly those associated with pregnancy.

For metabolomic analysis, plasma samples stored at −80 °C were thawed on ice and vortexed for 10 s. A total of 50 μL of each sample was mixed with 300 μL of extraction solution (acetonitrile: methanol = 1:4, v/v) containing internal standards. The mixture was vortexed for 3 min and centrifuged at 12,000 rpm for 10 min at 4 °C. Subsequently, 200 μL of the supernatant was collected and incubated at −20 °C for 30 min, followed by centrifugation at 12,000 rpm for 3 min (4 °C). Finally, 180 μL of the supernatant was transferred for LC–MS analysis. Metabolomic profiling was performed using a UPLC–MS/MS platform (ExionLC AD coupled with a QTRAP™ 6500+ system). Chromatographic separation was carried out on a Waters ACQUITY UPLC HSS T3 C18 column (1.8 μm, 2.1 mm × 100 mm) at 40 °C with a flow rate of 0.4 mL/min and an injection volume of 2 μL. The mobile phases consisted of water (0.1% formic acid, phase A) and acetonitrile (0.1% formic acid, phase B), with the following gradient program: 5% B to 20% B within 2 min, increased to 60% B over 3 min, increased to 99% B within 1 min and held for 1.5 min, then returned to 5% B within 0.1 min and equilibrated for 2.4 min. Mass spectrometry analysis was performed using a triple quadrupole-linear ion trap mass spectrometer (QTRAP® LC–MS/MS system) equipped with an ESI Turbo Ion-Spray interface, operating in both positive and negative ion modes. The source parameters were set as follows: source temperature 500 °C; ion spray voltage 5500 V (positive mode) and −4500 V (negative mode); ion source gas I, gas II, and curtain gas were set to 55, 60, and 25 psi, respectively; collision gas was set to high. Instrument tuning and mass calibration were performed

using polypropylene glycol solutions. Data acquisition was conducted in multiple reaction monitoring (MRM) mode, with specific MRM transitions optimized for each metabolite. Metabolite identification and annotation were performed based on MS/MS spectral matching using a self-built MWDB database, combined with retention time and fragmentation pattern information. Quantification of metabolites was achieved using the MRM mode based on peak area integration, and data processing was carried out using Analyst (v1.6.3) and MultiQuant (v3.0.3) software.

Subsequently, WGCNA of metabolite abundance was performed using the "WGCNA (v1.73)" package in R (v4.3.2)[71]. Specifically, outlier samples were identified and removed by hierarchical clustering analysis. The scale-free topology fit index (R^2) was calculated across a range of soft-thresholding powers, and the optimal soft threshold (β) was selected when R^2 reached 0.8 to construct a scale-free network. A one-step network construction method was used, setting the minimum module size to 30 metabolites, and modules with similar expression patterns were merged. Module eigengenes (MEs) were then calculated, and correlations between MEs and phenotypic data (rectal temperature) were analyzed. Metabolites within significant modules showing an absolute correlation coefficient (|GS |) greater than 0.4 with the phenotype and a module membership (MM) greater than 0.6 were defined as metabolites associated with rectal temperature.

For differential metabolite analysis, 40 Huaxi cattle with similar gestational stages, good health status, and no close genetic relationships were selected from the cohort of 111 animals. These individuals were divided into two groups based on rectal temperature: a non-heat stress (NHS) group ($n = 20$, rectal temperature ≤ 38.7 °C) and a heat stress (HS) group ($n = 20$, rectal temperature ≥39.3 °C). OPLS-DA was performed using SIMCA software and the "ropls" R package to identify metabolites that discriminated between the two groups while removing variation unrelated to heat stress[72]. Differential metabolites were defined using the following criteria: variable importance in projection (VIP) > 1, $|\log_2 FC| > 0.5$, and $P < 0.05$.

Overlapping metabolites from WGCNA and differential analyses were prioritized based on Pearson correlation coefficients (WGCNA package) with rectal temperature, with the top 30 designated as thermal-responsive MMTs. Pathway enrichment of MMTs was analyzed through MetaboAnalyst 6.0 using the KEGG database.

Whole genome sequencing and GWAS analysis

To investigate genetic variation underlying heat stress–related metabolites, no additional whole-genome sequencing was performed for the present study. Genome-wide association analyses were conducted using previously published WGS data from the same 111 adult Huaxi cows analyzed in the plasma metabolomic study[73]. These WGS data were originally generated and reported in our prior study and are reused here solely for integrative analyses with newly generated metabolomic data[73]. By explicitly integrating these existing genomic datasets with the newly generated metabolomic data, we addressed research questions distinct from those examined in the prior publication, which focused on growth-stage–specific traits.

Raw sequencing reads were quality-filtered using fastp (v0.23.2) with default settings, and the clean reads were subsequently aligned to the Bos taurus reference genome (ARS-UCD2.0, NCBI assembly accession GCF_002263795.3) using BWA-MEM (v0.7.17-r1188). CNVs were identified using CNVcaller[74], retaining variants with silhouette score >0.65 and minor allele frequency > 0.05 to minimize false positives. GWAS was conducted through GAPIT3 using six analytical models: GLM, MLM, CMLM, FarmCPU, MLMM, and BLINK[75]. To control for population structure and relatedness, the first five principal components (PC1–PC5) and the kinship matrix were included as covariates in the GWAS model. Genome-wide significance thresholds were established via Bonferroni correction ($P < 0.05/N$, $N = 33{,}078$). Candidate CNVs were annotated using ANNOVAR, with flanking genes defined as those located within ±50 kb of each variant[76]. Functional enrichment analyses were performed using KOBAS 3.0 platform (http://bioinfo.org/kobas), incorporating GO terms and KEGG pathway annotations.

To further evaluate the functional relevance of CNV loci identified through metabolite-based GWAS, the sample size was expanded to the full cohort ($n = 202$) to improve the robustness and accuracy of the analyses. Genotypes of candidate CNVs were extracted from previously published WGS data of these 202 Huaxi cattle. Associations between CNV genotypes and previously collected growth-related traits—including body weight, body conformation traits, backfat thickness, and longissimus dorsi muscle area—were examined across all 202 individuals to assess the potential genetic effects of CNVs on growth performance. In addition, under heat stress conditions, physiological parameters (rectal temperature, heart rate, and respiratory rate) were compared among adult cattle with different CNV genotypes within the same cohort ($n = 202$) to evaluate the potential genetic contribution of candidate CNVs to heat stress adaptation. All statistical analyses were conducted using R software (v4.3.2). Differences among genotypes were assessed by one-way analysis of variance (ANOVA). Data are presented as mean ± standard error of the mean (SEM), and statistical significance was defined as a two-sided $P < 0.05$.

Construction of transcriptomic expression profiles based on public datasets

To investigate the roles of candidate genes in heat stress response and developmental regulation in cattle, we obtained publicly available RNA-seq datasets from the Sequence Read Archive (https://www.ncbi.nlm.nih.gov/). These included eight tissue types (blood, subcutaneous fat, longissimus dorsi muscle, liver, hypothalamus, pituitary gland, mammary gland, rumen) from both heat stressed and control cattle, along with data from longissimus dorsi muscle of 36 thermoneutral cattle (18 young [~1 year] and 18 adult [~2.5 years] animals) representing two developmental stages (Supplementary Data 1). Data processing and bioinformatic analyses followed established methods[73]. Specifically, the raw data were processed using fastp (v0.23.2), and ribosomal RNA was removed using Bowtie2 (v2.3.5.1) to obtain high-quality clean reads. These clean reads were aligned to the Bos taurus reference genome (ARS-UCD2.0, NCBI assembly accession GCF_002263795.3) using HISAT2 (v2.1.0). Transcript assembly and quantification were performed using StringTie (v2.1.1). Analysis of gene expression differences was performed using DESeq2 (v1.26.0). DEGs between groups were considered significant if they met the criteria of $|\log_2(FC)| > 0.5$ and a false discovery rate (FDR) < 0.01.

Cultivation of primary bovine skeletal muscle cells and establishment of heat stress models

The isolation and identification of the primary SMSCs were carried out by referring to the methods described in the previous study[77]. Briefly, skeletal muscle tissues were washed with PBS containing 1% streptomycin, minced into small pieces, and sequentially digested with collagenase and trypsin. The resulting cell suspension was filtered through 70 μm and 40 μm nylon meshes and seeded into culture flasks maintained at 37 °C in a humidified atmosphere with 5% CO_2. SMSCs were purified by density gradient centrifugation once cultures reached ~80% confluency.

The identity of SMSCs was confirmed by immunofluorescence staining for Pax7. Cells were fixed with 4% paraformaldehyde for 30 min, permeabilized with 0.5% Triton X-100 for 20 min, and blocked with 10% goat serum for 1 h at room temperature. Subsequently, cells were incubated overnight at 4 °C with an anti-Pax7 antibody (1:200) under gentle agitation, followed by incubation with a fluorophore-conjugated secondary antibody for 2 h in the dark. Nuclei were counterstained with DAPI for 1 min, and images were captured using an inverted fluorescence microscope.

To determine optimal heat stress conditions, SMSCs in the logarithmic growth phase were exposed to different temperature gradients (37 °C, 39 °C, 40.5 °C, and 42 °C) for various durations (1 h, 3 h, 6 h, 9 h, and 12 h), with three biological replicates per treatment. Quantitative PCR analysis of *HSP70* and *HSP60* expression revealed maximal induction at 42 °C for 3 h, which was selected for subsequent experiments. Thermoneutral cells (37 °C) served as controls. All heat treatments were performed in standard CO_2 incubators (5% CO_2) with controlled humidity.

Overexpression and interference with vector construction as well as cell transfection

Overexpression and knockdown adenoviruses targeting *CIITA* (Gene ID: XM_010819255.4; shRNA sequence: ACGAGGTCCTCAGTTACATTG) were constructed by Hanbio (Shanghai, China) using the pAdEasy-EF1α-MCS-3×FLAG-CMV-EGFP and pAdEasy-U6-CMV-EGFP vectors. The shRNA sequence was designed and verified by BLAST to ensure specificity against cattle *CIITA*. Viral packaging was performed in 293 A cells using the Adeasy system, and viral titers were determined by TCID50 assay.

Primary bovine SMSCs were infected at 40–50% confluence with an optimized multiplicity of infection of 24. Infection was carried out in half the usual culture medium volume for 4 h to enhance viral adsorption, after which the medium volume was restored and replaced with complete growth medium after 16 h of total incubation. Infection efficiency was evaluated 48 h post-infection via EGFP fluorescence microscopy and further confirmed by qPCR analysis of target gene expression.

Determination and analysis of cell transcriptome and metabolome

To investigate the role of *CIITA* under heat stress conditions, SMSCs overexpressing *CIITA* (HS + OE-*CIITA*) and corresponding negative control cells (HS + OE-NC) were established and subjected to heat stress at 42 °C for 3 h, thereby generating a *CIITA* overexpressing SMSCs heat stress model. Total RNA was extracted using RNAiso Plus reagent (TaKaRa, Japan) following the manufacturer's instructions. The RNA-seq libraries were constructed using the VAHTS mRNA-seq V8 Kit (Vazyme, China) and sequenced on the DNBSEQ-T7 platform (MGI Tech, China). The bioinformatics analyses were performed following the same pipeline as described for the tissue RNA-seq data. DEGs were identified based on the criteria of $|\log_2(FC)| > 0.2$ and FDR < 0.05, and protein–protein interaction networks were constructed using the STRING database[78].

For metabolomic profiling, targeted metabolomics analysis was conducted on *CIITA* overexpressing SMSCs under heat stress (Wuhan Metwell Biotechnology, China). Differential metabolites were defined using the thresholds of VIP > 1, $|\log_2(FC)| > 0.3$, and FDR < 0.05.

Detection of cell viability, cell proliferation, cell cycle and ATP

To further determine the biological effects of *CIITA* overexpression under heat stress, HS + OE-*CIITA* and HS + OE-NC SMSCs were treated under the same heat stress conditions (42 °C for 3 h). Cell viability was assessed in treated and control groups using the Cell Counting Kit-8 (Solarbio, China), and the optical density was measured at 450 nm using a microplate reader. Cell proliferation was evaluated using the BeyoClick™ EdU Cell Proliferation Kit with Alexa Fluor 594 (Beyotime, China). Fluorescence images were acquired using an inverted fluorescence microscope (Leica, Germany) and analyzed with ImageJ software. Cell cycle distribution was assessed by flow cytometry using the Cell Cycle Analysis Kit (Beyotime, China). After propidium iodide staining, cells were analyzed on a CytoFLEX flow cytometer (Beckman Coulter, USA) equipped with a 488-nm excitation laser and a 585/21-nm emission filter. Data acquisition was performed using CytExpert software (v2.4), and the proportions of cells in the G0/G1, S, and G2/M phases were quantified with ModFit LT (v5.0). Cellular ATP levels were determined using the ATP Content Assay Kit (Servicebio, China) according to the manufacturer's instructions. All experimental operations were performed strictly following the manufacturers' protocols.

RNA extraction and qPCR analysis

Total RNA was extracted using RNAiso Plus reagent (TaKaRa, Japan) following the manufacturer's protocol. Briefly, 1 mL of RNAiso Plus was added to each culture dish or well, and the lysate was incubated at room temperature for 5 min. After the addition of 200 μL of chloroform, samples were vigorously shaken for 15 s and centrifuged at 12,000 rpm for 15 min at 4 °C. The aqueous phase was transferred to a new tube, mixed with an equal volume of pre-chilled isopropanol, and centrifuged again at 12,000 rpm for 10 min to obtain RNA pellets. The pellets were washed twice with 75% DEPC-treated ethanol, air-dried, dissolved in 20 μL of DEPC-treated water, and stored at −80 °C until use.

Complementary DNA (cDNA) was synthesized using the PrimeScript™ FAST RT Reagent Kit (TaKaRa, Japan) according to the manufacturer's protocol. QPCR primers were designed using the Primer3Plus online tool (https://www.primer3plus.com/) based on sequences retrieved from the NCBI nucleotide database, and synthesized by Wuhan Tianyi Huiyuan Biological Technology Co., Ltd. (Wuhan, China; Supplementary Table 2). QPCR was performed using the TB Green Premix Ex Taq II (FAST) Kit (TaKaRa, Japan) with gene-specific primers. Amplification was carried out under the following conditions: 95 °C for 10 min, followed by 40 cycles of 95 °C for 15 s, 60 °C for 30 s, and 72 °C for 30 s. Relative transcript levels were calculated using the $2^{-\Delta\Delta Ct}$ method, with *ACTB* serving as the internal reference gene for normalization.

Copy number variation validation

To verify the identified CNVs, overlapping genomic regions were assessed and visualized using the Integrative Genomics Viewer[79]. QPCR was subsequently performed for experimental validation[80]. Genomic DNA was extracted from peripheral blood using the TIANamp Genomic DNA Kit (TIANGEN, China) according to the manufacturer's protocol. Specific primers targeting the candidate CNV region (CHR25:9,557,000–9,605,500 bp) were designed with Primer3Plus (https://www.primer3plus.com/) based on the Bos taurus reference genome sequence. QPCR assays were conducted using the TB Green Premix Ex Taq II (FAST) Kit (TaKaRa, Japan) under the following thermal cycling conditions: 95 °C for 10 min, followed by 40 cycles of 95 °C for 15 s, 60 °C for 30 s, and 72 °C for 30 s. All reactions were performed in triplicate. Relative CNV copy numbers were quantified using the $2^{-\Delta\Delta Ct}$ method, with *ACTB* as the internal reference gene. Primer sequences used for CNV validation are listed in Supplementary Table 2.

Statistics and reproducibility

All quantitative data in this study are presented as mean ± SEM. To ensure a uniform scale for comparison, all experimental results, which included three to eight biological replicates (encompassing cell viability ($n = 7$), cell proliferation ($n = 6$), ATP content ($n = 4$), cell cycle distribution ($n = 4$), and relative gene expression via qPCR), were first normalized to their respective control groups. Statistical significance of differences between groups was analyzed using GraphPad Prism software (version 8.0). Following normalization, an unpaired, two-tailed t-test was employed. Statistical significance was defined as "*" $P < 0.05$ and "**" $P < 0.01$. All graphs were generated using GraphPad Prism 8.0 to visually present the normalized data and significance markers.

Ethics approval

All animal procedures were approved by the Institutional Animal Care and Use Committee of Southwest University (Approval No. IACUC-20221128-02).

Reporting summary

Further information on research design is available in the Nature Portfolio Reporting Summary linked to this article.

Data availability

The WGS data generated in our previous study and the RNA-seq data produced in the present study have been deposited in the NCBI database under accession numbers PRJNA1164013 and PRJNA1261581, respectively[73]. All tissue RNA-seq datasets used in this study were obtained from publicly available datasets in the NCBI database; detailed sample information, including accession numbers and original publication citations, is provided in Supplementary Data 1. Source data underlying all figures are provided in the Supplementary Data 2. The gating strategy for Fig. 6i is presented in Supplementary Fig. 4. All other data, including the raw

metabolomics data, are available from the corresponding author upon reasonable request.

Received: 10 June 2025; Accepted: 20 April 2026;
Published online: 02 May 2026

References

1. Rahimi, J., Mutua, J. Y., Notenbaert, A. M. O., Marshall, K. & Butterbach-Bahl, K. Heat stress will detrimentally impact future livestock production in East Africa. *Nat. Food* **2**, 88–96 (2021).
2. Du, H. et al. Exacerbated heat stress induced by urban browning in the Global South. *Nat. Cities* **2**, 157–169 (2025).
3. Brasier, N. et al. The molecular signature of heat stress in sweat reveals non-invasive biomarker candidates for health monitoring. *Commun. Biol.* **8**, 15 (2025).
4. Hansen, P. J. Physiological and cellular adaptations of zebu cattle to thermal stress. *Anim. Reprod. Sci.* **82-83**, 349–360 (2004).
5. Periard, J. D., Eijsvogels, T. M. H. & Daanen, H. A. M. Exercise under heat stress: thermoregulation, hydration, performance implications, and mitigation strategies. *Physiol. Rev.* **101**, 1873–1979 (2021).
6. Koch, F. et al. Heat stress directly impairs gut integrity and recruits distinct immune cell populations into the bovine intestine. *Proc. Natl. Acad. Sci. USA* **116**, 10333–10338 (2019).
7. Mousavi, F., Karimi-Dehkordi, S., Kargar, S. & Ghaffari, M. H. Effect of chromium supplementation on growth performance, meal pattern, metabolic and antioxidant status and insulin sensitivity of summer-exposed weaned dairy calves. *Animal* **13**, 968–974 (2019).
8. Halli, K., Cohrs, I., Bruegemann, K., Koch, C. & Koenig, S. Effects of temperature-humidity index on blood metabolites of German dairy cows and their female calves. *J. Dairy. Sci.* **106**, 7281–7294 (2023).
9. Mota, C. M. D. & Madden, C. J. Neural circuits of long-term thermoregulatory adaptations to cold temperatures and metabolic demands. *Nat. Rev. Neurosci.* **25**, 143–158 (2024).
10. Febbraio, M. A. Alterations in energy metabolism during exercise and heat stress. *Sports Med.* **31**, 47–59 (2001).
11. Liao, Y. et al. Metabolomics profiling of serum and urine in three beef cattle breeds revealed different levels of tolerance to heat stress. *J. Agric. Food Chem.* **66**, 6926–6935 (2018).
12. Abbas, Z. et al. Glucose metabolism and dynamics of facilitative Glucose Transporters (GLUTs) under the influence of heat stress in dairy cattle. *Metabolites* **10**, 19 (2020).
13. Lin, L. et al. l-Theanine attenuates heat stress-induced proteotoxicity and alterations in carbohydrate and lipid metabolism via heat shock factor 1. *Food Funct.* **14**, 6172–6186 (2023).
14. Valenstein, M. L. et al. Structure of the nutrient-sensing hub GATOR2. *Nature* **607**, 610 (2022).
15. Wang, Y. et al. S-allyl cysteine ameliorates heat stress-induced oxidative stress by activating Nrf2/HO-1 signaling pathway in BMECs. *Toxicol. Appl. Pharmacol.* **416**, 10 (2021).
16. Gai, Z. et al. L-arginine alleviates heat stress-induced mammary gland injury through modulating CASTOR1-mTORC1 axis mediated mitochondrial homeostasis. *Sci. Total Environ.* **926**, 13 (2024).
17. Chen, Y. et al. Genomic atlas of the plasma metabolome prioritizes metabolites implicated in human diseases. *Nat. Genet.* **55**, 44 (2023).
18. Shin, S. et al. An atlas of genetic influences on human blood metabolites. *Nat. Genet.* **46**, 543–550 (2014).
19. Sun, C. et al. Mapping recurrent mosaic copy number variation in human neurons. *Nat. Commun.* **15**, 4220 (2024).
20. Harris, L. et al. Genome-wide association testing beyond SNPs. *Nat. Rev. Genet.* **26**, 156–170 (2025).
21. Lee, H. et al. Genome-wide copy number variation study reveals KCNIP1 as a modulator of insulin secretion. *Genomics* **104**, 113–120 (2014).
22. Liu, F. et al. Targeting VPS72 inhibits ACTL6A/MYC axis activity in HCC progression. *Hepatology* **78**, 1384–1401 (2023).
23. Lu, Y. et al. Integrated analysis of copy number variation-associated lncRNAs identifies candidates contributing to the etiologies of congenital kidney anomalies. *Commun. Biol.* **6**, 16 (2023).
24. Kerr, E. M., Gaude, E., Turrell, F. K., Frezza, C. & Martins, C. P. Mutant Kras copy number defines metabolic reprogramming and therapeutic susceptibilities. *Nature* **531**, 110 (2016).
25. Jo, J. H., Nejad, J. G., Kim, H. R. & Lee, H. G. Effect of seven days heat stress on feed and water intake, milk characteristics, blood parameters, physiological indicators, and gene expression in Holstein dairy cows. *J. Therm. Biol.* **123**, 103929 (2024).
26. Dahl, G. E., Tao, S. & Monteiro, A. P. A. Effects of late-gestation heat stress on immunity and performance of calves. *J. Dairy. Sci.* **99**, 3193–3198 (2016).
27. Liu, Y. et al. Selenogenome and AMPK signal insight into the protective effect of dietary selenium on chronic heat stress-induced hepatic metabolic disorder in growing pigs. *J. Anim. Sci. Biotechnol.* **12**, 68 (2021).
28. Enkler, L. et al. Arf1 coordinates fatty acid metabolism and mitochondrial homeostasis. *Nat. Cell Biol.* **25**, 1157 (2023).
29. McCoin, C. S., Knotts, T. A. & Adams, S. H. Acylcarnitines-old actors auditioning for new roles in metabolic physiology. *Nat. Rev. Endocrinol.* **11**, 617–625 (2015).
30. Lee, J., Ellis, J. M. & Wolfgang, M. J. Adipose fatty acid oxidation is required for thermogenesis and potentiates oxidative stress-induced inflammation. *Cell Rep.* **10**, 266–279 (2015).
31. Angelini, A. et al. PHDs/CPT1B/VDAC1 axis regulates long-chain fatty acid oxidation in cardiomyocytes. *Cell Rep.* **37**, 109767 (2021).
32. Hagenbeek, F. A. et al. Heritability estimates for 361 blood metabolites across 40 genome-wide association studies. *Nat. Commun.* **11**, 1 (2020).
33. Zheng, Y. et al. Effects of selenium as a dietary source on performance, inflammation, cell damage, and reproduction of livestock induced by heat stress: a review. *Front. Immunol.* **12**, 820853 (2021).
34. Hannan, F. M. et al. Endocrine effects of heat exposure and relevance to climate change. *Nat. Rev. Endocrinol.* **20**, 673–684 (2024).
35. Chiang, W. C., Ching, T. T., Lee, H. C., Mousigian, C. & Hsu, A. O. L. HSF-1 regulators DDL-1/2 link insulin-like signaling to heat-shock responses and modulation of longevity. *Cell* **148**, 322–334 (2012).
36. Kim, J. et al. TFEB-GDF15 axis protects against obesity and insulin resistance as a lysosomal stress response. *Nat. Metab.* **3**, 410–427 (2021).
37. Liu, L. et al. Intra-islet alpha-cell Gs signaling promotes glucagon release. *Nat. Commun.* **15**, 5129 (2024).
38. Xie, G. et al. Skeletal muscle and hepatic insulin signaling is maintained in heat-stressed lactating Holstein cows. *J. Dairy. Sci.* **99**, 4032–4042 (2016).
39. Jing, S. et al. SUMOylated Golgin45 associates with PML-NB to transcriptionally regulate lipid metabolism genes during heat shock stress. *Commun. Biol.* **7**, 532 (2024).
40. Korobkina, E. D. et al. Brown fat ATP-citrate lyase links carbohydrate availability to thermogenesis and guards against metabolic stress. *Nat. Metab.* **6**, 2187–2202 (2024).
41. Staruschenko, A., Alexander, R. T., Caplan, M. J. & Ilatovskaya, D. V. Calcium signalling and transport in the kidney. *Nat. Rev. Nephrol.* **20**, 541–555 (2024).
42. Sammad, A. et al. Investigation of metabolome underlying the biological mechanisms of acute heat stressed granulosa cells. *Int. J. Mol. Sci.* **23**, 2146 (2022).
43. Jiang, Q. et al. Impact of a Saccharomyces cerevisiae fermentation product during an intestinal barrier challenge in lactating Holstein cows on ileal microbiota and markers of tissue structure and immunity. *J. Anim. Sci.* **101**, 16 (2023).
44. Matos, A. R., Mendes, A. T., Scotti-Campos, P. & Arrabaca, J. D. Study of the effects of salicylic acid on soybean mitochondrial lipids

and respiratory properties using the alternative oxidase as a stress-reporter protein. *Physiol. Plant.* **137**, 485–497 (2009).
45. Zalutskaya, Z., Lapina, T. & Ermilova, E. The Chlamydomonas reinhardtii alternative oxidase 1 is regulated by heat stress. *Plant Physiol. Biochem.* **97**, 229–234 (2015).
46. Cardenas-Monroy, C. A. et al. The mitochondrial alternative oxidase Aox1 is needed to cope with respiratory stress but dispensable for pathogenic development in Ustilago maydis. *PLoS ONE* **12**, e0173389 (2017).
47. Liu, Y. et al. In-depth transcriptome profiling of Cherry Valley duck lungs exposed to chronic heat stress. *Front. Vet. Sci.* **11**, 1417244 (2024).
48. Suksa-Ard, P., Nuanlaong, S., Pooljun, C., Azzeme, A. M. & Suraninpong, P. Decoding the transcriptomics of oil palm seed germination. *Plants*. **13**, 2680 (2024).
49. Adhikari, A. et al. IFN-gamma and *CIITA* modulate IL-6 expression in skeletal muscle. *Cytokine X* **2**, 100023 (2020).
50. Liu, Y. et al. Chronic heat stress promotes liver inflammation in broilers via enhancing NF-kappaB and NLRP3 signaling pathway. *BMC Vet. Res.* **18**, 289 (2022).
51. Munoz-Canoves, P., Scheele, C., Pedersen, B. K. & Serrano, A. L. Interleukin-6 myokine signaling in skeletal muscle: a double-edged sword?. *Febs J.* **280**, 4131–4148 (2013).
52. Ting, J. P. Y. & Trowsdale, J. Genetic control of MHC class II expression. *Cell* **109**, S21–S33 (2002).
53. Burhans, W. S., Burhans, C. A. R. & Baumgard, L. H. Invited review: lethal heat stress: the putative pathophysiology of a deadly disorder in dairy cattle. *J. Dairy. Sci.* **105**, 3716–3735 (2022).
54. Zhu, X. S. & Ting, J. A 36-amino-acid region of *CIITA* is an effective inhibitor of CBP: Novel mechanism of gamma interferon-mediated suppression of collagen α 2 (I) and other promoters. *Mol. Cell. Biol.* **21**, 7078–7088 (2001).
55. Liu, X. et al. The structural basis of protein acetylation by the p300/CBP transcriptional coactivator. *Nature* **451**, 846–850 (2008).
56. Fujita, H., Aratani, S. & Nakajima, T. Grap2 cyclin D interacting protein negatively regulates CREB-binding protein, inhibiting fibroblast-like synoviocyte growth. *Mol. Med. Rep.* **23**, 8 (2021).
57. Chen, Y. et al. A conserved phosphorylation site within the forkhead domain of FoxM1B is required for its activation by cyclin-CDK1. *J. Biol. Chem.* **284**, 30695–30707 (2009).
58. Trinh, A. T., Kim, S. H. & Chang, H. E. Y. Cyclin-dependent Kinase 1-dependent phosphorylation of cAMP response element-binding protein decreases chromatin occupancy. *J. Biol. Chem.* **288**, 23765–23775 (2013).
59. Gao, C. et al. Downregulating CREBBP inhibits proliferation and cell cycle progression and induces daunorubicin resistance in leukemia cells. *Mol. Med. Rep.* **22**, 2905–2915 (2020).
60. Lee, B. H. & Mathews, M. B. Transcriptional coactivator cAMP response element binding protein mediates induction of the human proliferating cell nuclear antigen promoter by the adenovirus E1A oncoprotein. *Proc. Natl. Acad. Sci. USA* **94**, 4481–4486 (1997).
61. Peng, A. et al. EZH2 promotes DNA replication by stabilizing interaction of POLδ and PCNA via methylation-mediated PCNA trimerization. *Epigenetics Chromatin* **11**, 14 (2018).
62. Habibi, P. et al. Effect of heat stress on DNA damage: a systematic literature review. *Int. J. Biometeorol.* **66**, 2147–2158 (2022).
63. Ghasemi, F. et al. High MHC-II expression in Epstein-Barr virus-associated gastric cancers suggests that tumor cells serve an important role in antigen presentation. *Sci. Rep.* **10**, 14786 (2020).
64. Mori, S. et al. Neoself-antigens are the primary target for autoreactive T cells in human lupus. *Cell* **187**, 6071–6087 (2024).
65. Yosef, O. et al. Metabolic reprogramming driven by Ant2 deficiency augments T Cell function and anti-tumor immunity in mice. *Nat. Commun.* **16**, 4292 (2025).
66. Wang, X., Zhang, S., Xue, D., Neculai, D. & Zhang, J. Metabolic reprogramming of macrophages in cancer therapy. *Trends Endocrinol. Metab.* **36**, 660–676 (2024).
67. Kao, Y. et al. Metabolic reprogramming of interleukin-17-producing gammadelta T cells promotes ACC1-mediated de novo lipogenesis under psoriatic conditions. *Nat. Metab*. **7**, 966–984 (2025).
68. Ryall, J. G. Metabolic reprogramming as a novel regulator of skeletal muscle development and regeneration. *Febs J.* **280**, 4004–4013 (2013).
69. Ryall, J. G. et al. The NAD (+)-dependent SIRT1 deacetylase translates a metabolic switch into regulatory epigenetics in skeletal muscle stem cells. *Cell Stem Cell* **16**, 171–183 (2015).
70. Scata, M. C. et al. Hyperthermia-induced changes in leukocyte survival and phagocytosis: a comparative study in bovine and buffalo leukocytes. *Front. Vet. Sci.* **10**, 1327148 (2023).
71. Langfelder, P. & Horvath, S. WGCNA: an R package for weighted correlation network analysis. *BMC Bioinform.* **9**, 559 (2008).
72. Idkowiak, J. et al. Best practices and tools in R and Python for statistical processing and visualization of lipidomics and metabolomics data. *Nat. Commun.* **16**, 8714 (2025).
73. Liu, C. et al. Genome-wide association integrating a transcriptomic meta-analysis suggests that genes related to fat deposition and muscle development are closely associated with growth in Huaxi Cattle. *Vet. Sci.* **12**, 13 (2025).
74. Wang, X. et al. CNVcaller: highly efficient and widely applicable software for detecting copy number variations in large populations. *Gigascience* **6**, 1–12 (2017).
75. Wang, J. & Zhang, Z. GAPIT Version 3: boosting power and accuracy for genomic association and prediction. *Genom. Proteom. Bioinform.* **19**, 629–640 (2021).
76. Wang, K., Li, M. & Hakonarson, H. ANNOVAR: functional annotation of genetic variants from high-throughput sequencing data. *Nucleic Acids Res.* **38**, e164 (2010).
77. Wang, X. et al. Integrative analysis of whole genome bisulfite and transcriptome sequencing reveals the effect of sodium butyrate on DNA methylation in the differentiation of bovine skeletal muscle satellite cells. *Genomics* **116**, 110959 (2024).
78. Szklarczyk, D. et al. STRING v11: protein-protein association networks with increased coverage, supporting functional discovery in genome-wide experimental datasets. *Nucleic Acids Res.* **47**, D607–D613 (2019).
79. Robinson, J. T. et al. Integrative genomics viewer. *Nat. Biotechnol.* **29**, 24–26 (2011).
80. Chew, S. et al. Homozygous deletion of the UGT2B17 gene is not associated with osteoporosis risk in elderly Caucasian women. *Osteoporos. Int.* **22**, 1981–1986 (2011).

Acknowledgements

The authors sincerely thank all staff members at Chongqing Jinxia Animal Husbandry Co., Ltd. for their valuable contributions to the collection of phenotypic data and blood samples from Huaxi cattle. This work was supported by National Natural Science Foundation of China (Grant No. 32573180), the Open Project of State Key Laboratory of Animal Biotech Breeding (Grant No. 2024SKLAB6-111), and Fundamental Research Funds for the Central University (Grant No. SWU-XDJH202301).

Author contributions

G.E., H.G., and C.L. conceived and designed the study. C.L., D.Y., and P.R. analyzed the sequencing data. Z.W., C.L., and D.H. carried out experiments. C.L. and G.E. wrote the paper. Y.H., L.Z., and S.C. reviewed and edited the manuscript. All authors read and approved the manuscript.

Competing interests

The authors declare no competing interests.

Additional information

Supplementary information The online version contains supplementary material available at https://doi.org/10.1038/s42003-026-10151-w.

Correspondence and requests for materials should be addressed to Huijiang Gao or Guangxin E.

Peer review information *Communications Biology* thanks Ravi Gandham, Manas Ranjan Shenhe Liu and Muhammed Elayadeth-Meethal for their contribution to the peer review of this work. Primary Handling Editor: David Favero. A peer review file is available.